ACS OMEGA

Open Access

http://pubs.acs.org/journal/acsodf

Article

Unraveling the Positive Role of WO_3 on Supported Vanadium Catalysts for NO_x Reduction by Operando Spectroscopy

Zhihui Lv, Guangyan Xu,* Yingjie Wang, Yunbo Yu, and Hong He

Cite This: *ACS Omega* 2025, 10, 358−367

Read Online

ACCESS | Metrics & More | Article Recommendations | Supporting Information

ABSTRACT: Selective catalytic reduction of nitrogen oxides (NO_x) by ammonia (NH_3−SCR) over supported vanadium catalysts is a commercial technology for NO_x abatement in combustion exhaust. The addition of tungsten oxide (WO_3) significantly enhances the performance of supported vanadium catalysts (V_2O_5/TiO_2), but the mechanism underlying this enhancement remains controversial. In this study, we employed combined operando spectroscopy (DRIFTS-UV−vis-MS) to investigate the dynamic state of active sites (acid sites and redox sites) on V_2O_5−WO_3/TiO_2 during the NH_3−SCR reaction. Our findings confirmed that WO_3 occupied the TiO_2 surface and reduced the available surface sites for V_2O_5 anchoring, thus promoting the agglomeration of vanadia species. This structural effect significantly improved the reducibility of VO_x on V_2O_5−WO_3/TiO_2 catalysts, consequently enhancing the efficiency for NO_x reduction. The heightened reducibility rendered the reoxidation of vanadia species a rate-limiting step, resulting in the presence of vanadia species in a lower oxidation state (V^{4+}) during the NH_3−SCR reaction.

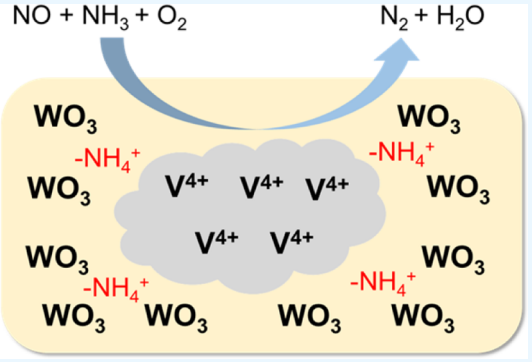

1. INTRODUCTION

Nitrogen oxides (NO_x) emitted from vehicles and power plants lead to environmental problems, such as photochemical smog, acid rain, and haze.[1−4] Selective catalytic reduction of NO_x by ammonia (NH_3−SCR) is a widely used technology for NO_x reduction in heavy-duty diesel vehicles and power plants.[5−9] The supported vanadium catalysts are the most important commercial SCR catalysts due to their superior catalytic activity and sulfur tolerance.[8,10−18] Moreover, the addition of WO_3 remarkably improves the capability of V_2O_5/TiO_2 catalysts in practical applications, boosting low-temperature activity, broadening the operational temperature range, improving N_2 selectivity, increasing resistance to toxicity, and enhancing thermal stability.[12,19−26]

Generally, there are two different types of active sites that participate in the NH_3−SCR reaction over V_2O_5/TiO_2 catalysts, which are acid sites and redox sites.[27−31] First, NH_3 adsorbs on the Lewis or Brønsted acid sites to form coordinated NH_3 or NH_4^+ cations, respectively, which further react with NO or adsorbed nitrates to produce NH_2NO or NH_4NO_2.[30−34] Subsequently, these intermediates decompose to generate N_2 and H_2O. Meanwhile, adsorbed NH_3 transfers an H atom to adjacent redox sites and reduces the vanadium species to a lower valence state (V^{4+}), which is further reoxidized to complete the redox cycle.[35−41] Recently, it was found that V═O could serve as both a redox site and an acid site in the NH_3−SCR reaction, and that NH_3 adsorption would suppress the redox cycle of V═O species.[42]

The promoting effect of WO_3 on supported V_2O_5/TiO_2 catalysts in the NH_3−SCR reaction has been extensively investigated.[16,19,20,43−46] Generally, two kinds of promotion effects, namely, structural and electronic effects, have been proposed for the promotion by WO_3. Jaegers and his coworkers[20] employed ^{51}V MAS NMR spectroscopy to reveal the structural effects of WO_3 on supported V_2O_5/TiO_2 catalysts. They proposed that unreactive WO_3 induces the generation of oligomeric vanadia species, which were proposed as the reactive sites for NO_x abatement. In contrast, based on EPR spectra and TPR profiles, Grunert et al.[46] suggested that WO_3 directly interacts with vanadium species and prevents the agglomeration of large surface vanadium oxide islands. Moreover, Li et al.[45] used Raman and TPR to research the effects of WO_3 on V_2O_5−WO_3/TiO_2 catalysts and observed that the dispersion of WO_3 on the titania surface significantly altered the acid characteristics and surface species on these catalysts. In contrast, Yang et al.[19] proposed that WO_3 addition increased the density and strength of Brønsted acid sites on vanadia catalysts, which were suggested to be the active components in NO_x reduction.

Received: July 9, 2024
Revised: September 26, 2024
Accepted: December 12, 2024
Published: December 23, 2024

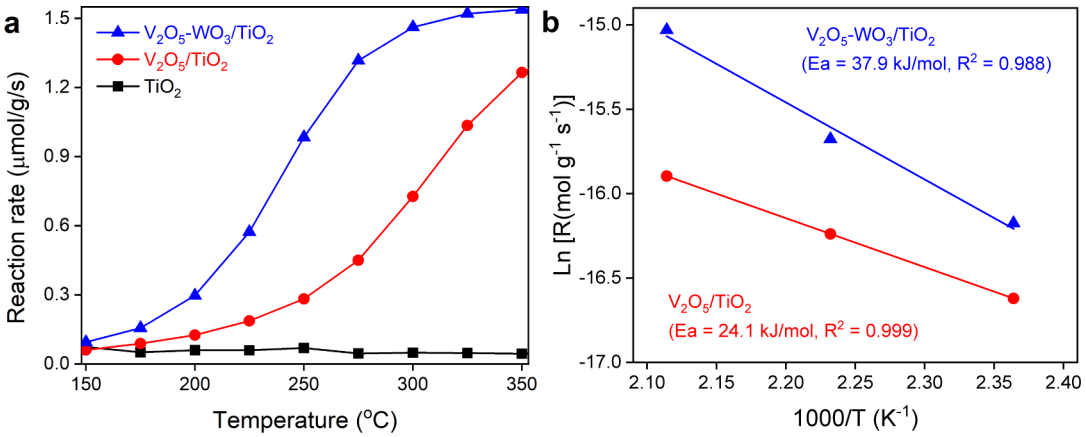

Figure 1. (a) Reaction rate for NO_x reduction over supported vanadium catalysts. (b) Arrhenius plots for the rate of NO_x reduction. Feed composition: 500 ppm of NO, 500 ppm of NH_3, 5% O_2, 1% H_2O, N_2 balance.

Despite intensive research, there is still debate regarding whether the promoting effect of WO_3 stems from structural or electronic effects. In this study, we employed combined operando spectroscopy (Diffuse reflectance infrared Fourier-transform spectroscopy−ultraviolet−visible spectroscopy−mass spectrometry, DRIFTS-UV−vis-MS)[42,47−49] to study the surface intermediates, active sites, and reaction products of the NH_3−SCR reaction over V_2O_5−WO_3/TiO_2 catalysts. This approach allowed us to resolve the promotion effect of WO_3 on these supported vanadium catalysts in this reaction. This study provides new insights for designing high-efficiency SCR catalysts, and the combined operando spectroscopy employed herein can be applied to the study of other heterogeneous catalytic reactions.

2. EXPERIMENTAL SECTION

2.1. Catalyst Preparation. Supported V_2O_5−WO_3/TiO_2 catalysts were prepared by a wet impregnation method.[28,50] Specifically, an appropriate volume of aqueous ammonium metavanadate or ammonium metatungstate was impregnated into a suspension of TiO_2 (Degussa P25) in water. After thorough mixing for 1 h, the water was evaporated in a rotary vacuum evaporator at 60 °C. Then, the samples were dried in an electric oven at 100 °C for 12 h and calcined at 450 °C for 5 h in a muffle furnace. As for the V_2O_5−WO_3/TiO_2 sample, the impregnation was repeated with the second component, ammonium metavanadate. Afterward, this sample was evaporated and calcined through the above steps. The V_2O_5 and WO_3 loadings on these catalysts were 2 and 10 wt %, respectively, if applicable.

2.2. Activity Tests. The activity tests were accomplished in a fixed-bed reactor with an inner diameter of 6 mm.[47] The reaction gas was comprised of 500 ppm of NO, 500 ppm of NH_3, 1% H_2O, and 5% O_2 in N_2 balance with a total flow rate of 500 mL min^{-1}(GHSV = 100,000 h^{-1}). 120 mg of sample with 40−60 mesh was used. The concentration of NO, NH_3, NO_2, and N_2O was analyzed by an FTIR spectrometer (Nicolet iS 10).[51] The conversions of NO_x and NH_3, and selectivity of N_2 were calculated according to eqs 13.

$$NO_x \text{ conversion} = \frac{[NO_x]_{in} - [NO_x]_{out}}{[NO_x]_{in}} \times 100\% \quad (1)$$

$$NH_3 \text{ conversion} = \frac{[NH_3]_{in} - [NH_3]_{out}}{[NH_3]_{in}} \times 100\% \quad (2)$$

$$N_2 \text{ selectivity} = \left(1 - \frac{2 \times [N_2O]_{out}}{[NO_x + NH_3]_{in} - [NO_x + NH_3]_{out}}\right) \times 100\% \quad (3)$$

where

$$NO_x = NO + NO_2$$

The kinetics experiments were performed in the above fixed-bed reactor, and the reaction gas was the same as the activity testes. Internal and external diffusion effects had been eliminated according to our previous works.[47,48] The NO_x and NH_3 conversions were kept below 20%. The Arrhenius plots for NO_x reduction were drawn, and the apparent activation energies were calculated. The reaction rate ($-R_{NOx}$) was calculated according to eq 4, where F_{NOx} and X_{NOx} represent the molar flow rate (mol s^{-1}) and NO_x conversion (%), respectively. W represents the sample weight (g).

$$-R_{NO_x} \text{ (mol/g/s)} = F_{NO_x} \times X_{NO_x}/W \quad (4)$$

2.3. Operando DRIFTS-MS. Operando diffuse reflectance infrared Fourier-transform spectroscopy (DRIFTS)−mass spectrometer (MS) experiments were carried out on an FTIR spectrometer (Nicolet iS 50).[48,49] A powder sample (70 mg) was placed in a Harrick Scientific cell controlled by a Harrick ATC Temperature Controller. Typical reaction components were 500 ppm of NO, 500 ppm of NH_3, 5% H_2O (when added), and 5% O_2 in an Ar balance (100 mL min^{-1}). Water vapor was supplied by passing the gas flow over a water bottle. The DRIFTS spectra were collected in the range of 650−4000 cm^{-1} with a resolution of 4 cm^{-1} and an accumulation of 100 scans. Moreover, an online mass spectrometer (InProcess Instruments, GAM 200) was directly connected to the reaction cell to monitor the gaseous product of N_2 (m/z = 28).

2.4. Operando DR-UV−vis. The ultraviolet−visible (UV−vis) experiment was conducted on a UV−vis spectrophotometer (PerkinElmer, LAMBDA 650) equipped with the Harrick Praying Mantis Attachment.[48,49] Sample powder (70 mg) was placed into a Harrick Scientific cell controlled by a Harrick ATC Temperature Controller. The reaction compo-

https://doi.org/10.1021/acsomega.4c06372
ACS Omega 2025, 10, 358−367

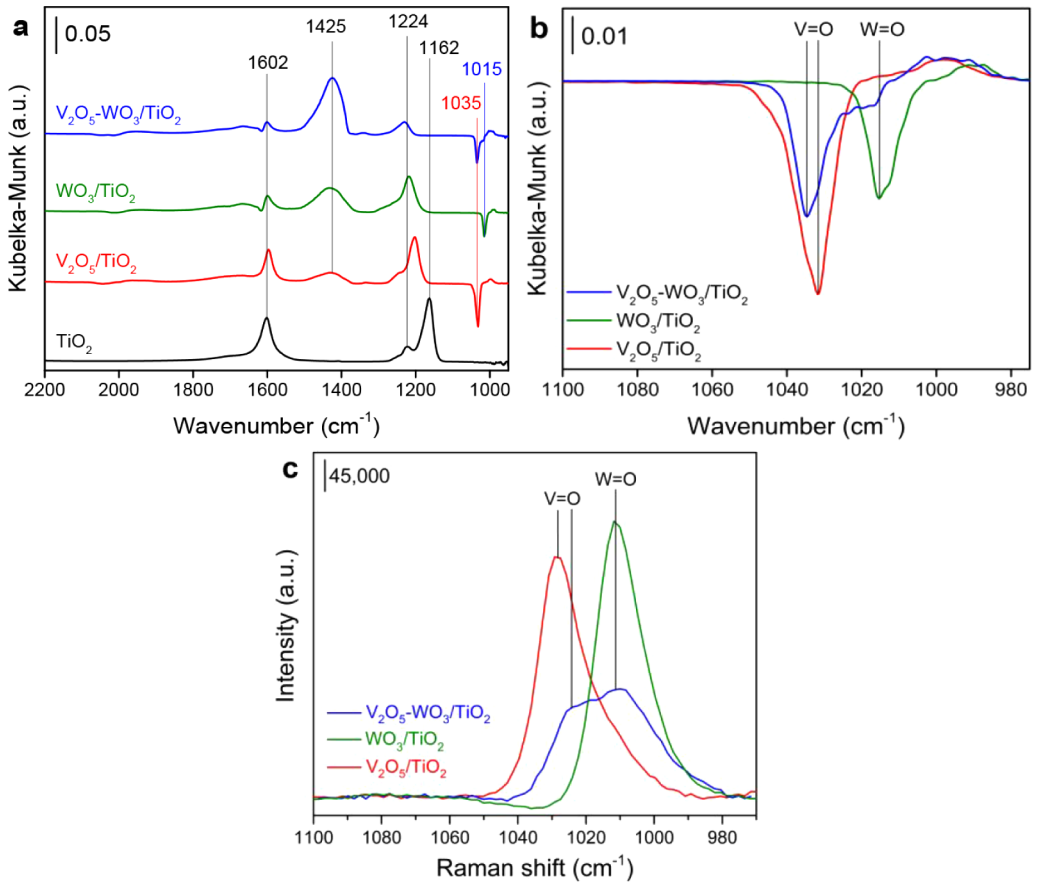

Figure 2. (a,b) DRIFTS spectra of NH_3 adsorption on V_2O_5–WO_3/TiO_2 at 200 °C. (c) Raman spectra of V_2O_5–WO_3/TiO_2 at 400 °C. Feed composition: (a,b) 500 ppm of NH_3 in Ar balance; (c) 10% O_2 in N_2 balance.

nents were 500 ppm of NO, 500 ppm of NH_3, and 5% O_2 in N_2 balance (100 mL min^{-1}). The spectra were collected in the range of 800–200 nm with a resolution of 1 nm. The DR-UV–vis data were collected by continuously measuring the absorbance at 700 nm with a time resolution of 1 s^{-1}.

2.5. Characterizations. The X-ray photoelectron spectra (XPS) were collected on an AXIS Supra spectrometer equipped with Al Kα radiation.[52] The charging effect of the samples was eliminated by using the energy value of C 1*s* (284.8 eV).

3. RESULTS

Supported vanadium catalysts were prepared using a wet impregnation method with TiO_2 (Degussa P25) as the support.[27,28,42] As shown in Figures 1 and S1, TiO_2 exhibited low activity in the NH_3–SCR reaction, achieving less than 5% of NO_x conversion at temperatures below 400 °C. In contrast, the V_2O_5/TiO_2 catalyst demonstrated significant activity for NO_x reduction at temperatures above 250 °C. Notably, the addition of WO_3 substantially enhanced the catalytic activity of V_2O_5/TiO_2, especially at low temperatures. At 250 °C, the NO_x conversion of V_2O_5–WO_3/TiO_2 was 62%, which was consistent with the literature.[53,54] Specifically, the reaction rate for NO_x reduction on V_2O_5–WO_3/TiO_2 (0.98 μmol g^{-1} s^{-1}) was 3.5 times higher than that on V_2O_5/TiO_2 (0.28 μmol g^{-1} s^{-1}) at 250 °C. Moreover, the apparent activation energy for NO_x reduction on V_2O_5–WO_3/TiO_2 (37.9 kJ mol^{-1}) was higher than that on V_2O_5/TiO_2 (24.1 kJ mol^{-1}),[17] but the reaction rate of V_2O_5–WO_3/TiO_2 was faster. This was because the reaction rate was not only affected by apparent activation energy but also influenced by the pre-exponential factor. And, the pre-exponential factor of the reaction reflected the collision frequency of the reaction, which was susceptible to the number of active sites and their intrinsic reactivity. Apparently, the pre-exponential factor of V_2O_5–WO_3/TiO_2 was larger than that of V_2O_5/TiO_2, which can be seen from Figure 1b that the vertical intercept of V_2O_5–WO_3/TiO_2 was larger compared to V_2O_5/TiO_2. Additionally, NH_3 conversion exhibited a trend similar to that of NO_x conversion, and the N_2 selectivity was approximately equal to 100% on these catalysts (Figure S1).

The acidic properties of supported vanadium catalysts were characterized by DRIFTS of NH_3 adsorption (Figure 2). The samples were pre-exposed to NH_3 at 200 °C for 2 h, followed by Ar purging for 30 min. Three peaks were observed for bare TiO_2, which were assigned to the asymmetric stretch (1602 cm^{-1}) and symmetric stretch (1224 and 1162 cm^{-1}) of NH_3 adsorbed on Ti sites.[27,55] In addition to the above peaks, another band (1425 cm^{-1}) was observed in the spectrum of V_2O_5/TiO_2, attributed to the symmetric deformation mode of NH_4^+ cations on Brønsted acid sites.[30] The Lewis acid sites on V_2O_5/TiO_2 consisted of Ti sites and V sites. Moreover, a negative peak (1035 cm^{-1}) assigned to the V=O stretching vibration was found for the V_2O_5/TiO_2.[42,56,57] The addition of WO_3 significantly increased the number of Brønsted acid sites on WO_3/TiO_2, accompanied by a decrease in the number of Lewis acid sites. Thus, the Lewis acid sites on WO_3/TiO_2 included Ti sites and WO_x sites. Similarly, a negative peak at 1015 cm^{-1} was observed on WO_3/TiO_2, assigned to the W=

https://doi.org/10.1021/acsomega.4c06372
ACS Omega 2025, 10, 358–367

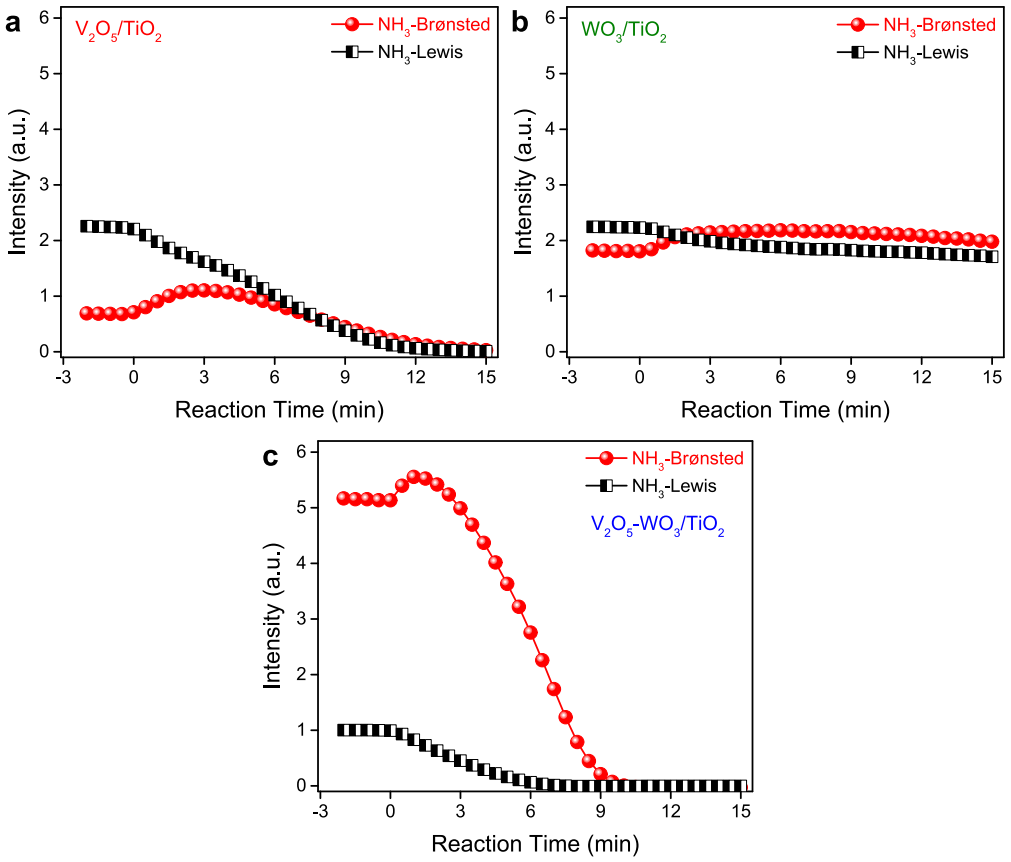

Figure 3. Reactivity of NH_3 adsorbed on different acid sites over (a) V_2O_5/TiO_2, (b) WO_3/TiO_2, and (c) V_2O_5–WO_3/TiO_2 catalysts. The samples were pre-exposed to NH_3 for 2 h, followed by Ar purging, and then exposed to NO + O_2 for 15 min. Feed composition: 500 ppm of NH_3, 500 ppm of NO, 5% of the O_2 in Ar balance, 200 °C.

O stretching vibration. On the V_2O_5–WO_3/TiO_2, the presence of V_2O_5 and WO_3 significantly enhanced the intensity of bands corresponding to Brønsted acid sites, while the number of Lewis acid sites was apparently decreased. In conclusion, the Lewis acid sites almost came from TiO_2, and the Brønsted acid sites completely originated from VO_x and WO_x. More importantly, WO_3 addition induced a blue-shift for the IR peak assigned to vanadia species (V═O) (Figure 2b), revealing the agglomeration of vanadia species on the V_2O_5–WO_3/TiO_2.[56,57] Furthermore, the Raman signal of V═O (1030 cm^{-1}) was observed on V_2O_5/TiO_2, and this signal was weakened on V_2O_5–WO_3/TiO_2 (Figure 2c), consistent with previous literature.[50] It confirmed that WO_3 addition induced the formation of polymeric vanadia species. This structural effect of WO_3 on the agglomeration of vanadia species was consistent with Jaegers' work,[20] in which oligomeric vanadia sites were suggested to act as the active sites for NO_x reduction.

Subsequently, the influence of water vapor on the acid sites of supported vanadium catalysts was further researched (Figure S2). Our previous work confirmed that water vapor could interact with the V═O site and induce the conversion from Lewis acid sites to Brønsted acid sites.[42] Lewandowska and his coworkers also proposed that the addition of water vapor resulted in the dissociative adsorption of water on V_2O_5/TiO_2, forming surface hydroxyl groups (V–OH) based on their DFT calculations and *in situ* Raman measurements.[58,59] In this work, the introduction of water vapor also remarkably enhanced the intensity of W–OH Brønsted acid sites on WO_3/TiO_2, leading to a decrease in Lewis acid sites (Figure S2a). Hence, water vapor could also interact with W═O (Lewis acid site) and convert them into W–OH (Brønsted acid site). Consequently, on the V_2O_5–WO_3/TiO_2, the bands corresponding to Brønsted acid sites were much more intense than those of Lewis acid sites, especially under wet conditions (Figure S2b).

The performance of NH_3 adsorbed on different acid sites was further evaluated by operando DRIFTS (Figures 3 and S3). The samples were pre-exposed to NH_3 for 2 h, followed by Ar purging, and then exposed to NO+O_2 for 15 min. The DRIFTS spectra were collected at 200 °C, considering that the reactivity of V_2O_5–WO_3/TiO_2 was too low to observe the change of adsorbed NH_3 species at temperatures below 200 °C. At temperatures above 250 °C, the reaction rates of surface NH_3 species were too fast, leading to hardly any observation of their change in the NH_3–SCR process. The peaks for NH_3 adsorbed on Lewis acid sites (NH_3–Lewis, 1310–1150 cm^{-1}) and Brønsted acid sites (NH_3–Brønsted, 1540–1310 cm^{-1}) were integrated (Figure S3). On the V_2O_5/TiO_2, the number of NH_3–Lewis was much greater than that of NH_3–Brønsted, and the NH_3–Lewis were gradually consumed after exposure to NO+O_2. Instead, the NH_3–Brønsted significantly increased in the first few minutes, followed by a continuous decrease for 15 min. This phenomenon was related to the transformation of Lewis acid sites to Brønsted acid sites under wet conditions, which had been confirmed in previous works.[42,60] On WO_3/TiO_2, the introduction of NO only induced a slight conversion between Lewis acid sites and Brønsted acid sites, while adsorbed NH_3 was hardly consumed. On V_2O_5–WO_3/TiO_2,

https://doi.org/10.1021/acsomega.4c06372
ACS Omega 2025, 10, 358–367

by contrast, the number of NH_3−Brønsted was much greater than that of NH_3−Lewis. Notably, both NH_3−Brønsted and NH_3−Lewis were rapidly consumed after exposure to NO + O_2, indicating their high reactivity for NO_x reduction. Meanwhile, the slight increase in the concentration of NH_3−Brønsted was attributed to the conversion of NH_3−Lewis, consistent with that occurring on V_2O_5/TiO_2. Therefore, it is hard to determine which acid sites show higher reactivity due to their easy interconversion. However, the presence of WO_3 did increase the number of acid sites and also promoted their reactivity, especially for the Brønsted acid sites.

The redox capabilities of supported vanadium catalysts were further investigated by operando DR-UV−vis experiments. UV−vis spectra showed that TiO_2 exhibited intense absorption only in the ultraviolet region (Figure S4). WO_3/TiO_2 showed a similar property to TiO_2, indicating that WO_3 had negligible influence. By contrast, V_2O_5/TiO_2 showed moderate absorbance in the visible region. Besides, the addition of WO_3 significantly enhanced the absorbance in the visible region. According to the literature,[27,28] the absorbance at 800−600 nm is due to the d-d transition of V^{4+}, whereas the absorbance at 400 nm is attributed to the charge transfer of V^{5+} ($O^{2-} \rightarrow V^{5+}$). During the operando DR-UV−vis experiment, the dynamic state of the vanadium species (V^{4+}) was investigated by monitoring the absorbance at 700 nm continuously. The absorbance (700 nm) on WO_3/TiO_2 remained unchanged during the CO reduction, revealing that neither TiO_2 nor WO_3 could affect this signal (Figure S5). Instead, CO reduction significantly enhanced the absorbance (700 nm) of V_2O_5/TiO_2, indicating that V^{5+} species were reduced to V^{4+}. Notably, the reduction was more intensive on V_2O_5−WO_3/TiO_2, revealing that WO_3 addition enhanced the redox properties of vanadia species.

On V_2O_5/TiO_2, the presence of NH_3 slowly reduced the vanadia species in the absence of NO (first state in Figure 4).

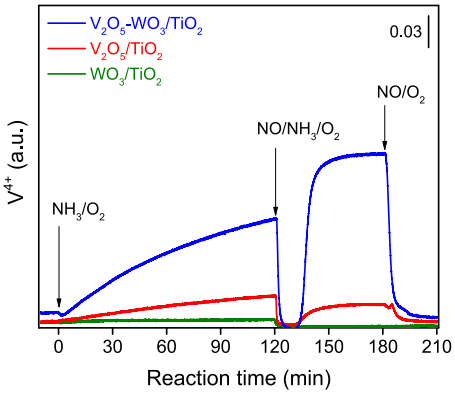

Figure 4. Operando DR-UV−vis experiment of a step-response NH_3−SCR reaction at 200 °C on supported vanadium catalysts. The samples were pretreated in air for 1 h at 400 °C and successively exposed to (1) NH_3/O_2 (0−120 min), (2) $NO/NH_3/O_2$ (120−180 min), and (3) NO/O_2 (180−210 min) at 200 °C.

These vanadia species were suddenly reoxidized once exposed to NO, followed by a gradual reduction to reach a balanced state (second state in Figure 4). WO_3/TiO_2 showed little change during the above gas switching process, revealing that neither TiO_2 nor WO_3 showed reactivity for NO_x reduction. On V_2O_5−WO_3/TiO_2, however, the introduction of NH_3 remarkably reduced the vanadia species. Notably, this reduction is much slower compared to the reduction observed during the NH_3−SCR reaction. When the feed was changed from NH_3/O_2 to $NO/NH_3/O_2$, these VO_x species were quickly oxidized. In the steady-state NH_3−SCR reaction (second state in Figure 4), vanadia species predominantly exist in the V^{4+} state, suggesting that the oxidation of the V^{4+} species occurred more slowly than the reduction of the V^{5+} species. Upon the removal of NH_3 (third state in Figure 4), the V^{4+} species gradually reoxidized within the first 6 min, indicating that both the oxidation and reduction of vanadia species were rapid on V_2O_5−WO_3/TiO_2. Clearly, WO_3 addition significantly enhanced the redox ability of vanadia species over V_2O_5−WO_3/TiO_2 in the NH_3−SCR process.

Moreover, a combined operando DRIFTS-UV−vis-MS experiment was performed to study the surface intermediates, active sites, and N_2 formation during the NH_3−SCR process (Figure 5). The samples were pretreated and successively exposed to different reaction atmospheres. On the V_2O_5/TiO_2, the number of NH_3−Lewis was higher than that of NH_3−Brønsted, while they exhibited little change during gas switching (Figure 5a). On the V_2O_5−WO_3/TiO_2 (Figure 5b), in contrast, the amount of NH_3−Brønsted was much more than that of NH_3−Lewis, though they also showed little change during the above processes. The vanadia species on these samples were rather different during the above step-response reaction. On V_2O_5/TiO_2, most vanadia species were in a higher valence state (V^{5+}) and remained stable during the above processes. In contrast, the vanadia species on V_2O_5−WO_3/TiO_2 were mostly in a lower valence state (V^{4+}). The results of XPS for V 2*p* (Figure S6) indicated that the vanadia species on V_2O_5/TiO_2 and V_2O_5−WO_3/TiO_2 were mainly present in V^{5+},[61] but it mostly existed in the form of V^{4+} on V_2O_5−WO_3/TiO_2 under the reaction conditions. It further proved that the addition of WO_3 induced the reduction of vanadia species under reaction atmospheres, thus enhancing the redox capability of V_2O_5/TiO_2 during the NH_3−SCR reaction. Notably, the increase in the NO concentration induced a remarkable oxidation of V^{4+} species (Figure 5c), which were subsequently reduced to their original level. Afterward, the vanadia species were only slightly influenced by the changes in O_2 and NH_3 concentrations and were suddenly oxidized upon the removal of NH_3. On V_2O_5/TiO_2, N_2 formation was significantly increased (from 140 to 220 ppm and from 150 to 200 ppm) when the concentrations of NO and O_2 were increased, though the surface intermediates and vanadia valence showed little change in this process. On the V_2O_5−WO_3/TiO_2, notably, N_2 formation was suddenly and greatly increased (from 310 to 500 ppm) by increasing the NO concentration, followed by a decrease to 410 ppm, consistent with the change in vanadia species. Similarly, increasing the O_2 concentration also enhanced the N_2 generation on this sample, while increasing the NH_3 concentration showed little effect on this reaction.

A combined operando DRIFTS-UV−vis-MS experiment was further conducted on V_2O_5−WO_3/TiO_2 to study the dynamic changes in surface intermediates, vanadia valence, and reaction products during the NH_3−SCR process (Figure 6). This sample was pre-exposed to a flow of $NO/NH_3/O_2$ for 2 h, and then different reactants (NO, NH_3, or NO+NH_3) were successively removed from the reaction stream. After the removal of NO (2nd step), both NH_3−Brønsted and V^{4+} species decreased, whereas N_2 formation rapidly stopped, revealing that gaseous NO mainly participated in the reaction

https://doi.org/10.1021/acsomega.4c06372
ACS Omega 2025, 10, 358−367

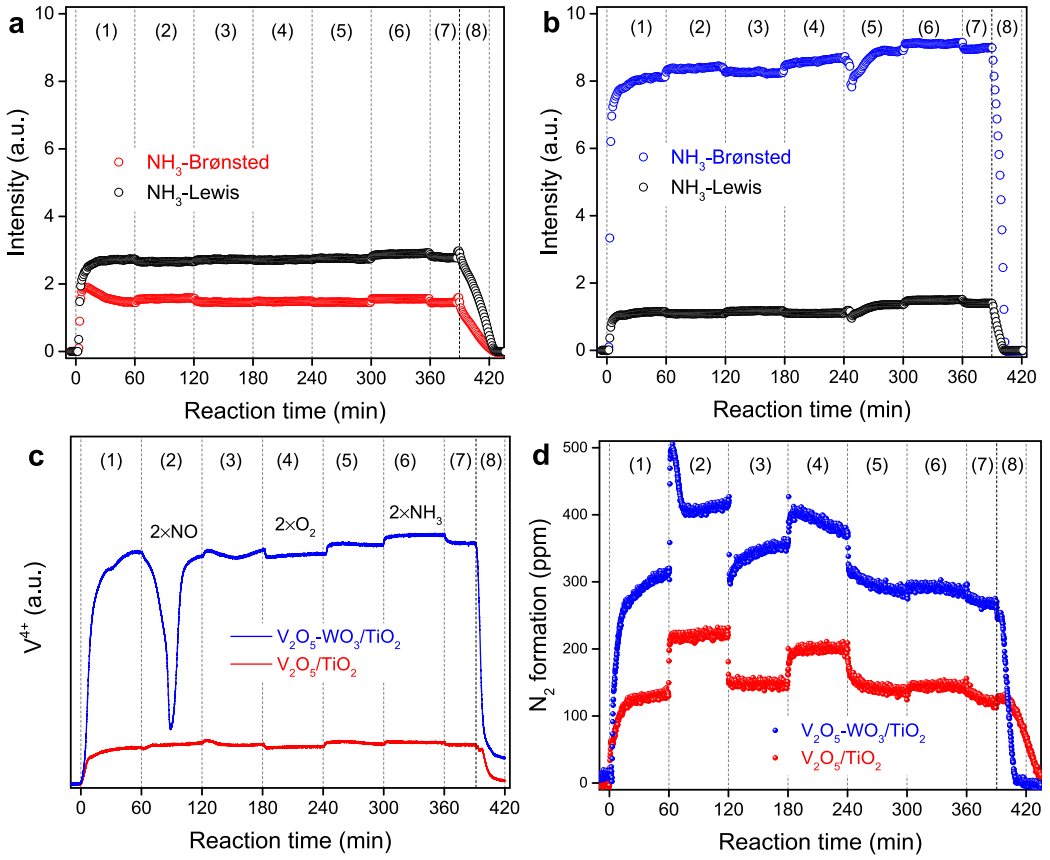

Figure 5. Dynamic change of adsorbed NH_3 on (a) V_2O_5/TiO_2, (b) $V_2O_5–WO_3/TiO_2$, (c) V^{4+} species, and (d) N_2 formation by operando DRIFTS-UV–vis-MS experiment during NH_3–SCR reaction. The samples were pretreated in O_2/Ar for 1 h at 400 °C and then cooled to 200 °C, followed by successive exposure to (1) $NO/NH_3/O_2$, (2) $2NO/NH_3/O_2$, (3) $NO/NH_3/O_2$, (4) $NO/NH_3/2O_2$, (5) $NO/NH_3/O_2$, (6) $NO/2NH_3/O_2$, (7) $NO/NH_3/O_2$, and (8) NO/O_2, respectively. Typical feed conditions: 500 ppm of NO, 500 ppm of NH_3, 5% of the O_2 in Ar balance. The "2" means 2 times of the reactant concentration (e.g., "2 × NO" refers to 1000 ppm of NO).

without adsorption. Meanwhile, the intensity of the NH_3–Lewis peaks increased slightly, possibly due to the conversion of NH_3–Brønsted. After the removal of NH_3 (4th step), both NH_3–Brønsted and NH_3-Lewis peaks decreased gradually, accompanied by the oxidation of V^{4+} species. However, the removal of gaseous NH_3 had little effect on the formation of N_2, indicating that this sample was saturated with excess adsorbed NH_3, which could maintain the NO_x reduction reaction for more than 10 min. Afterward, the introduction of NO (5th step) resulted in the rapid reduction of V^{5+} species within the first 3.5 min, which occurred faster than the oxidation of V^{4+} species observed in the fourth step. Subsequently, the removal of NO and NH_3 induced a remarkable decrease in the NH_3–Brønsted and V^{4+} species (6th step), while the introduction of reactants could rapidly restore the reaction. Afterward, NO and NH_3 were successively removed, which induced a continuous decrease in the NH_3–Brønsted and V^{4+} species (8th and 9th steps). In contrast, the addition of NO induced the rapid consumption of adsorbed NH_3 to generate N_2 as well as the rapid oxidation of V^{4+} species (10th step). Notably, the V^{4+} species showed precisely the same trend as NH_3–Brønsted during the above procedures, revealing the presence of adsorbed NH_3 on the V^{4+}–OH Brønsted acid sites. Besides, NH_3 adsorption appeared to suppress the oxidation of these V^{4+} species, which has also been observed on V_2O_5/TiO_2.[42] In contrast, NO could react with these adsorbed NH_3 and help restore the V^{4+} species. Notably, the vanadia species were mainly present in a lower valence state (V^{4+}) during this reaction, indicating that the reoxidation of V^{4+} species was the rate-limiting step of this reaction.

4. DISCUSSION

On supported V_2O_5/TiO_2 catalysts, both Ti sites and V sites can serve as Lewis acid sites for NH_3 adsorption, and V–OH groups can act as Brønsted acid sites to coordinate with NH_3 and form NH_4^+ cations. WO_3 addition remarkably increased the number of Brønsted acid sites on $V_2O_5–WO_3/TiO_2$, contributed by W–OH sites, accompanied by a significant decrease in Lewis acid sites. Similar to vanadia species, moisture could also induce the conversion of W═O (Lewis acid sites) to W–OH (Brønsted acid sites), thus remarkably increasing the number of Brønsted acid sites. On V_2O_5/TiO_2, both Lewis acid sites and Brønsted acid sites participated moderately in NO reduction, while their reactivity was hard to determine due to the interconversion of them, which was induced by water vapor.

Operando DR-UV–vis confirmed that the presence of WO_3 significantly enhanced the reducibility of vanadia species on the $V_2O_5–WO_3/TiO_2$, which was likely related to the formation of polymeric vanadyl species.[42,62] Moreover, the adsorption of NH_3 on Brønsted acid sites would suppress the oxidation of V^{4+}–OH possibly due to the steric effect (Figure 6), which has been confirmed in our previous work.[42]

https://doi.org/10.1021/acsomega.4c06372
ACS Omega 2025, 10, 358–367

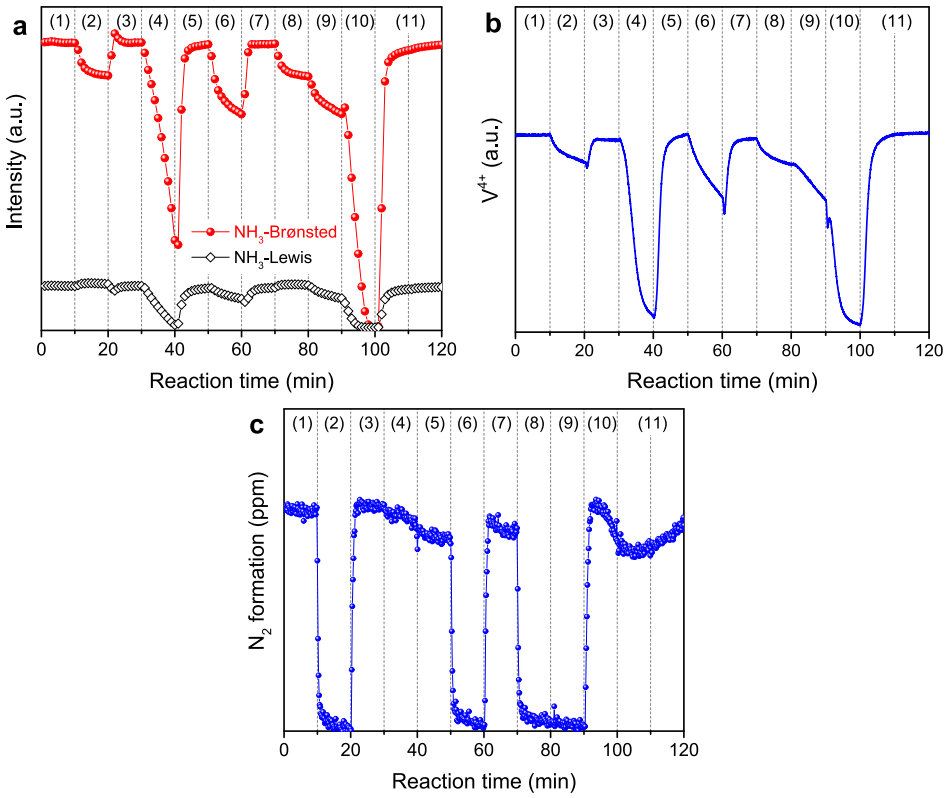

Figure 6. Dynamic changes in (a) adsorbed NH_3, (b) vanadia species, and (c) N_2 formation during operando DRIFTS-UV−vis-MS experiment of step−response NH_3−SCR reaction. The sample was pre-exposed to $NO/NH_3/O_2$ at 200 °C for 2 h and then successively exposed to (1) $NO/NH_3/O_2$, (2) NH_3/O_2, (3) $NO/NH_3/O_2$, (4) NO/O_2, (5) $NO/NH_3/O_2$, (6) O_2, (7) $NO/NH_3/O_2$, (8) NH_3/O_2, (9) O_2, (10) NO/O_2, and (11) $NO/NH_3/O_2$, respectively. Typical conditions: 500 ppm of NO, 500 ppm of NH_3, and 5% of the O_2 in an Ar balance.

Consequently, the valence state of vanadia species was sensitive to the NO concentration such that NO could react with the NH_3 adsorbed on V^{4+}−OH, thus releasing the V^{4+}−OH sites, ultimately inducing the rapid oxidation of V^{4+} species (Figure 5c). During the step−response experiment (Figure 6), the removal of gaseous NH_3 induced the gradual consumption of adsorbed NH_3 over a period of 10 min, while the formation of N_2 was hardly affected. If the NH_3 adsorbed on WO_3 directly participated in the NO_x reduction, the decrease in adsorbed NH_3 would induce a gradual decrease in N_2 formation. Rather, it was speculated that WO_3 served as a pool for NH_3 adsorption, which maintained the high efficiency of the catalyst for NO_x reduction. Moreover, as WO_3 provides active sites for NH_3 adsorption, more vanadia species could be released to serve as redox sites, thus contributing to the improved catalytic activity. Another possibility was interactions between neighboring tungsten and vanadia species, such as induction and conjugation.[46]

On the V_2O_5/TiO_2, the vanadia species were mainly present in a higher oxidation state (V^{5+}) in the NH_3−SCR process, indicating that their reduction was slow. On V_2O_5−WO_3/TiO_2, however, the vanadia species were mainly present in a lower oxidation state (V^{4+}), attributed to the superior reducibility of vanadia species. The increase in the NO concentration induced a remarkable boost in N_2 generation. The increase in O_2 concentration greatly enhanced N_2 formation, while it only slightly promoted the oxidation of vanadia species, indicating that the dehydrogenation was extremely fast and the reoxidation of V^{4+} species was the rate-limiting step on this sample under NH_3−SCR conditions.

5. CONCLUSIONS

The promotion effect of WO_3 on NH_3−SCR over supported vanadium catalysts was researched by combined operando spectroscopy. WO_3 occupied the surface of TiO_2, reducing the available surface sites for vanadia anchoring and inducing the agglomeration of vanadia species. This structural effect significantly enhanced the reducibility of vanadia species on V_2O_5−WO_3/TiO_2, thus greatly improving the efficiency of NO_x reduction. Furthermore, the increased reducibility made the reoxidation of vanadia species the rate-limiting step, resulting in their presence in a lower oxidation state (V^{4+}) during the NH_3−SCR reaction. Moreover, the addition of WO_3 greatly increased the number of Brønsted acid sites on V_2O_5−WO_3/TiO_2, especially in the presence of water vapor.

■ ASSOCIATED CONTENT

Supporting Information

The Supporting Information is available free of charge at https://pubs.acs.org/doi/10.1021/acsomega.4c06372.

Catalytic activity of vanadia catalysts, DRIFTS spectra, UV−vis spectra, and XPS spectra (PDF)

■ AUTHOR INFORMATION

Corresponding Author

Guangyan Xu − *State Key Joint Laboratory of Environment Simulation and Pollution Control, Research Center for Eco-Environmental Sciences, Chinese Academy of Sciences, Beijing 100085, China; University of Chinese Academy of Sciences,*

https://doi.org/10.1021/acsomega.4c06372
ACS Omega 2025, 10, 358−367

Beijing 100049, China; orcid.org/0000-0002-4275-7517; Email: gyxu@rcees.ac.cn

Authors

Zhihui Lv − *State Key Joint Laboratory of Environment Simulation and Pollution Control, Research Center for Eco-Environmental Sciences, Chinese Academy of Sciences, Beijing 100085, China; University of Chinese Academy of Sciences, Beijing 100049, China*

Yingjie Wang − *State Key Joint Laboratory of Environment Simulation and Pollution Control, Research Center for Eco-Environmental Sciences, Chinese Academy of Sciences, Beijing 100085, China;* orcid.org/0000-0002-6393-763X

Yunbo Yu − *State Key Joint Laboratory of Environment Simulation and Pollution Control, Research Center for Eco-Environmental Sciences, Chinese Academy of Sciences, Beijing 100085, China; University of Chinese Academy of Sciences, Beijing 100049, China; Center for Excellence in Regional Atmospheric Environment, Institute of Urban Environment, Chinese Academy of Sciences, Xiamen 361021, China;* orcid.org/0000-0003-2935-0955

Hong He − *State Key Joint Laboratory of Environment Simulation and Pollution Control, Research Center for Eco-Environmental Sciences, Chinese Academy of Sciences, Beijing 100085, China; University of Chinese Academy of Sciences, Beijing 100049, China; Center for Excellence in Regional Atmospheric Environment, Institute of Urban Environment, Chinese Academy of Sciences, Xiamen 361021, China;* orcid.org/0000-0001-8476-8217

Complete contact information is available at: https://pubs.acs.org/10.1021/acsomega.4c06372

Author Contributions

The manuscript was written through the contributions of all authors. All authors have approved the final version of the manuscript.

Notes

The authors declare no competing financial interest.

■ ACKNOWLEDGMENTS

This work was financially supported by the National Key R&D Program of China (2022YFC3704400), the National Natural Science Foundation of China (22276203), and the project of eco-environmental technology for carbon neutrality (RCEES-TDZ-2021-6).

■ REFERENCES

(1) Anenberg, S. C.; Miller, J.; Minjares, R.; Du, L.; Henze, D. K.; Lacey, F.; Malley, C. S.; Emberson, L.; Franco, V.; Klimont, Z.; Heyes, C. Impacts and mitigation of excess diesel-related NOx emissions in 11 major vehicle markets. *Nature* **2017**, *545*, 467−471.

(2) Richter, A.; Burrows, J. P.; Nuss, H.; Granier, C.; Niemeier, U. Increase in tropospheric nitrogen dioxide over China observed from space. *Nature* **2005**, *437*, 129−132.

(3) Chu, B. W.; Ma, Q. X.; Liu, J.; Ma, J. Z.; Zhang, P.; Chen, T. Z.; Feng, Q. C.; Wang, C. Y.; Yang, N.; Ma, H. N.; Ma, J. J.; Russell, A. G.; He, H. Air pollutant correlations in China: secondary air pollutant responses to NO_x and SO_2 control. *Environ. Sci. Technol. Lett* **2020**, *7*, 695−700.

(4) Wu, P. J.; Tang, X. G.; He, Z. H.; Liu, Y. X.; Wang, Z. H. Alkali metal poisoning and regeneration of selective catalytic reduction denitration catalysts: recent advances and future perspectives. *Energy Fuels* **2022**, *36* (11), 5622−5646.

(5) Granger, P.; Parvulescu, V. I. Catalytic NO_x abatement systems for mobile sources: from three-way to lean burn after-treatment technologies. *Chem. Rev* **2011**, *111*, 3155−3207.

(6) Parvulescu, V. I.; Grange, P.; Delmon, B. Catalytic removal of NO. *Catal. Today* **1998**, *46*, 233−316.

(7) Xu, G.; Shan, W.; Yu, Y.; Shan, Y.; Wu, X.; Wu, Y.; Zhang, S.; He, L.; Shuai, S.; Pang, H.; Jiang, X.; Zhang, H.; Guo, L.; Wang, S.; Xiao, F.-S.; Meng, X.; Wu, F.; Yao, D.; Ding, Y.; Yin, H.; He, H. Advances in emission control of diesel vehicles in China. *J. Environ. Sci* **2023**, *123*, 15−29.

(8) Lian, Z. H.; Li, Y. J.; Shan, W. P.; He, H. Recent progress on improving low-temperature activity of vanadia-based catalysts for the selective catalytic reduction of NO_x with ammonia. *Catalysts* **2020**, *10*, 1421.

(9) Wang, S.; Liu, J.; Jin, Z. S.; Guo, S. Q.; Cheng, D. H.; Deng, J.; Zhang, D. S. Gas-phase regeneration of metal-poisoned V_2O_5-WO_3/TiO_2 NH_3-SCR catalysts via a masking and reconstruction strategy. *Environ. Sci. Technol* **2024**, *58* (30), 13574−13584.

(10) Kwak, J. H.; Tonkyn, R. G.; Kim, D. H.; Szanyi, J.; Peden, C. H. F. Excellent activity and selectivity of Cu-SSZ-13 in the selective catalytic reduction of NO_x with NH_3. *J. Catal* **2010**, *275*, 187−190.

(11) Beale, A. M.; Gao, F.; Lezcano-Gonzalez, I.; Peden, C. H. F.; Szanyi, J. Recent advances in automotive catalysis for NO_x emission control by small-pore microporous materials. *Chem. Soc. Rev* **2015**, *44*, 7371−7405.

(12) Busca, G.; Lietti, L.; Ramis, G.; Berti, F. Chemical and mechanistic aspects of the selective catalytic reduction of NO_x by ammonia over oxide catalysts: a review. *Appl. Catal., B* **1998**, *18*, 1−36.

(13) Lai, J. K.; Wachs, I. E. A perspective on the selective catalytic reduction (SCR) of NO with NH_3 by supported V_2O_5-WO_3/TiO_2 catalysts. *ACS Catal* **2018**, *8*, 6537−6551.

(14) Han, L.; Cai, S.; Gao, M.; Hasegawa, J. Y.; Wang, P.; Zhang, J.; Shi, L.; Zhang, D. Selective catalytic reduction of NO_x with NH_3 by using novel catalysts: state of the art and future prospects. *Chem. Rev* **2019**, *119*, 10916−10976.

(15) Shan, W. P.; Yu, Y. B.; Zhang, Y.; He, G. Z.; Peng, Y.; Li, J. H.; He, H. Theory and practice of metal oxide catalyst design for the selective catalytic reduction of NO_x with NH_3. *Catal. Today* **2021**, *376*, 292−301.

(16) He, Y. Y.; Ford, M. E.; Zhu, M. H.; Liu, Q. C.; Tumuluri, U.; Wu, Z. L.; Wachs, I. E. Influence of catalyst synthesis method on selective catalytic reduction (SCR) of NO by NH_3 with V_2O_5-WO_3/TiO_2 catalysts. *Appl. Catal., B* **2016**, *193*, 141−150.

(17) Chen, G. D.; Chen, J. J.; Chen, X. P.; Yin, R. Q.; Li, K. Z.; Li, J. H. Monolith or powder: improper sample pretreatment may mislead the understanding of industrial V_2O_5-WO_3/TiO_2 catalysts operated in stationary resources. *Environ. Sci. Technol* **2022**, *56* (22), 16394−16399.

(18) Kim, S. I.; Choi, Y. J.; Lee, M. S.; Lee, D. H. Nitration-promoted vanadate catalysts for low-temperature selective catalytic reduction of NO_x with NH_3. *ACS Omega* **2023**, *8* (37), 34152−34159.

(19) Chen, J. P.; Yang, R. T. Role of WO_3 in mixed V_2O_5-WO_3/TIO_2 catalysis for selective catalytic reduciton of nitric-oxide with ammonia. *Appl. Catal., A* **1992**, *80*, 135−148.

(20) Jaegers, N. R.; Lai, J. K.; He, Y.; Walter, E.; Dixon, D. A.; Vasiliu, M.; Chen, Y.; Wang, C. M.; Hu, M. Y.; Mueller, K. T.; Wachs, I. E.; Wang, Y.; Hu, J. Z. Mechanism by which tungsten oxide promotes the activity of supported V_2O_5/TiO_2 catalysts for NO_x abatement: structural effects revealed by V^{51} MAS NMR spectroscopy. *Angew. Chem., Int. Ed* **2019**, *58*, 12609−12616.

(21) Inomata, Y.; Kubota, H.; Hata, S.; Kiyonaga, E.; Morita, K.; Yoshida, K.; Sakaguchi, N.; Toyao, T.; Shimizu, K.-I.; Ishikawa, S.; Ueda, W.; Haruta, M.; Murayama, T. Bulk tungsten-substituted vanadium oxide for low-temperature NO_x removal in the presence of water. *Nat. Commun* **2021**, *12* (1), 557.

(22) Wang, Y.; Yi, W.; Zeng, Y. J.; Chang, H. Z. Novel methods for assessing the SO_2 poisoning effect and thermal regeneration

possibility of MO_x-WO_3/TiO_2 (M = Fe, Mn, Cu, and V) catalysts for NH_3-SCR. *Environ. Sci. Technol* **2020**, *54*, 12612−12620.
(23) Wang, X.; Du, X.; Liu, S.; Yang, G.; Chen, Y.; Zhang, L.; Tu, X. Understanding the deposition and reaction mechanism of ammonium bisulfate on a vanadia SCR catalyst: a combined DFT and experimental study. *Appl. Catal., B* **2020**, *260*, 118168.
(24) Marberger, A.; Elsener, M.; Nuguid, R. J. G.; Ferri, D.; Krocher, O. Thermal activation and aging of a V_2O_3/WO_3-TiO_2 catalyst for the selective catalytic reduction of NO with NH_3. *Appl. Catal., A* **2019**, *573*, 64−72.
(25) Xu, L. W.; Wang, C. Z.; Chang, H. Z.; Wu, Q. R.; Zhang, T.; Li, J. H. New Insight into SO_2 poisoning and regeneration of CeO_2-WO_3/TiO_2 and V_2O_5-WO_3/TiO_2 catalysts for low-temperature NH_3-SCR. *Environ. Sci. Technol* **2018**, *52*, 7064−7071.
(26) Yu, W.; Wu, X.; Si, Z.; Weng, D. Influences of impregnation procedure on the SCR activity and alkali resistance of V_2O_5-WO_3/TiO_2 catalyst. *Appl. Surf. Sci* **2013**, *283*, 209−214.
(27) Zhu, M.; Lai, J.-K.; Tumuluri, U.; Wu, Z.; Wachs, I. E. Nature of active sites and surface intermediates during SCR of NO with NH_3 by supported V_2O_5-WO_3/TiO_2 catalysts. *J. Am. Chem. Soc* **2017**, *139* (44), 15624−15627.
(28) Marberger, A.; Ferri, D.; Elsener, M.; Krocher, O. The significance of Lewis acid sites for the selective catalytic reduction of nitric oxide on vanadium-based catalysts. *Angew. Chem., Int. Ed* **2016**, *55* (39), 11989−11994.
(29) He, G.; Lian, Z.; Yu, Y.; Yang, Y.; Liu, K.; Shi, X.; Yan, Z.; Shan, W.; He, H. Polymeric vanadyl species determine the low-temperature activity of V-based catalysts for the SCR of NOx with NH_3. *Sci. Adv* **2018**, *4* (11), No. eaau4637.
(30) Topsoe, N.-Y. Mechanism of the Selective Catalytic Reduction of Nitric Oxide by Ammonia Elucidated by in Situ On-Line Fourier Transform Infrared Spectroscopy. *Science* **1994**, *265* (5176), 1217−1219.
(31) Nuguid, R. J. G.; Ferri, D.; Marberger, A.; Nachtegaal, M.; Krocher, O. Modulated excitation Raman spectroscopy of V_2O_5/TiO_2: mechanistic insights into the selective catalytic reduction of NO with NH_3. *ACS Catal* **2019**, *9* (8), 6814−6820.
(32) Arnarson, L.; Falsig, H.; Rasmussen, S. B.; Lauritsen, J. V.; Moses, P. G. A complete reaction mechanism for standard and fast selective catalytic reduction of nitrogen oxides on low coverage VO_x/TiO_2(001) catalysts. *J. Catal* **2017**, *346*, 188−197.
(33) Yao, H. C.; Chen, Y.; Zhao, Z.; Wei, Y. C.; Liu, Z. C.; Zhai, D.; Liu, B. J.; Xu, C. M. Periodic DFT study on mechanism of selective catalytic reduction of NO via NH_3 and O_2 over the V_2O_5 (001) surface: competitive sites and pathways. *J. Catal* **2013**, *305*, 67−75.
(34) Mason, M. M.; Lee, Z. R.; Vasiliu, M.; Wachs, I. E.; Dixon, D. A. Initial steps in the selective catalytic reduction of NO with NH_3 by TiO_2-supported vanadium oxides. *ACS Catal* **2020**, *10* (23), 13918−13931.
(35) Zhu, M.; Lai, J. K.; Tumuluri, U.; Ford, M. E.; Wu, Z.; Wachs, I. E. Reaction pathways and kinetics for selective catalytic reduction (SCR) of acidic NO_x emissions from power plants with NH_3. *ACS Catal* **2017**, *7* (12), 8358−8361.
(36) Ek, M.; Ramasse, Q. M.; Arnarson, L.; Moses, P. G.; Helveg, S. Visualizing atomic-scale redox dynamics in vanadium oxide-based catalysts. *Nat. Commun* **2017**, *8* (1), 305.
(37) Godiksen, A. L.; Rasmussen, S. B. Identifying the presence of $[V = O]^{2+}$ during SCR using in-situ Raman and UV Vis spectroscopy. *Catal. Today* **2019**, *336*, 45−49.
(38) Doronkin, D. E.; Benzi, F.; Zheng, L.; Sharapa, D. I.; Amidani, L.; Studt, F.; Roesky, P. W.; Casapu, M.; Deutschmann, O.; Grunwaldt, J.-D. NH_3-SCR over V−W/TiO_2 investigated by operando X-ray absorption and emission spectroscopy. *J. Phys. Chem. C* **2019**, *123*, 14338−14349.
(39) Arnarson, L.; Falsig, H.; Rasmussen, S. B.; Lauritsen, J. V.; Moses, P. G. The reaction mechanism for the SCR process on monomer V^{5+} sites and the effect of modified Brønsted acidity. *Phys. Chem. Chem. Phys* **2016**, *18* (25), 17071−17080.
(40) Arnarson, L.; Rasmussen, S. B.; Falsig, H.; Lauritsen, J. V.; Moses, P. G. Coexistence of square pyramidal structures of Oxo vanadium (+5) and (+4) species over low-coverage VO_x/TiO_2 (101) and (001) anatase catalysts. *J. Phys. Chem. C* **2015**, *119* (41), 23445−23452.
(41) Zhang, J. Y.; Miao, J. F.; Huang, B. Y.; Chen, Y. T.; Chen, J. S.; Wang, J. X. Effect of carious acid anions on potassium poisoning and the mechanism of commercial V_2O_5-WO_3/TiO_2 catalysts for SCR of NO_x. *Ind. Eng. Chem. Res* **2024**, *63* (5), 2167−2176.
(42) Xu, G.; Li, H.; Yu, Y.; He, H. Dynamic change of active sites of supported vanadia catalysts for selective catalytic reduction of nitrogen oxides. *Environ. Sci. Technol* **2022**, *56* (6), 3710−3718.
(43) Xiao, X.; Xiong, S.; Li, B.; Geng, Y.; Yang, S. Role of WO_3 in NO reduction with NH_3 over V_2O_5-WO_3/TiO_2: a new insight from the kinetic study. *Catal. Lett* **2016**, *146* (11), 2242−2251.
(44) He, Y.; Ford, M. E.; Zhu, M.; Liu, Q.; Wu, Z.; Wachs, I. E. Selective catalytic reduction of NO by NH_3 with WO_3-TiO_2 catalysts: influence of catalyst synthesis method. *Appl. Catal., B* **2016**, *188*, 123−133.
(45) Wang, C.; Yang, S.; Chang, H.; Peng, Y.; Li, J. Dispersion of tungsten oxide on SCR performance of V_2O_5-WO_3/TiO_2: Acidity, surface species and catalytic activity. *Chem. Eng. J* **2013**, *225*, 520−527.
(46) Kompio, P.; Bruckner, A.; Hipler, F.; Auer, G.; Loffler, E.; Grunert, W. A new view on the relations between tungsten and vanadium in V_2O_5-WO_3/TiO_2 catalysts for the selective reduction of NO with NH_3. *J. Catal* **2012**, *286*, 237−247.
(47) Xu, G.; Ma, J.; Wang, L.; Lv, Z.; Wang, S.; Yu, Y.; He, H. Mechanism of the H_2 effect on NH_3-selective catalytic reduction over Ag/Al_2O_3: kinetic and diffuse reflectance infrared fourier transform spectroscopy studies. *ACS Catal* **2019**, *9* (11), 10489−10498.
(48) Xu, G. Y.; Zhang, Y.; Lin, J. G.; Wang, Y. B.; Shi, X. Y.; Yu, Y. B.; He, H. Unraveling the mechanism of ammonia selective catalytic oxidation on Ag/Al_2O_3 catalysts by operando spectroscopy. *ACS Catal* **2021**, *11* (9), 5506−5516.
(49) Xu, G.; Wang, H.; Yu, Y.; He, H. Role of silver species in H_2-NH_3-SCR of NO_x over Ag/Al_2O_3 catalysts: operando spectroscopy and DFT calculations. *J. Catal* **2021**, *395*, 1−9.
(50) Zhu, M. H.; Lai, J. K.; Tumuluri, U.; Wu, Z. L.; Wachs, I. E. Nature of active sites and surface intermediates during SCR of NO with NH_3 by supported V_2O_5-WO_3/TiO_2 catalysts. *J. Am. Chem. Soc* **2017**, *139* (44), 15624−15627.
(51) Xu, G. Y.; Ma, J. Z.; Wang, L.; Xie, W.; Liu, J. J.; Yu, Y. B.; He, H. Insight into the origin of sulfur tolerance of Ag/Al_2O_3 in the H_2-C_3H_6-SCR of NO_x. *Appl. Catal., B* **2019**, *244*, 909−918.
(52) Gillot, S.; Tricot, G.; Vezin, H.; Dacquin, J. P.; Dujardin, C.; Granger, P. Induced effect of tungsten incorporation on the catalytic properties of $CeVO_4$ systems for the selective reduction of NO_x by ammonia. *Appl. Catal., B* **2018**, *234*, 318−328.
(53) Lv, Z.; He, G. Z.; Ge, Y. L.; Liu, Y. C.; Yu, Y. B.; He, H. Effects of WO_3 and MoO_3 loadings on vanadia-based catalysts for NH_3-SCR: revealed by infrared and two-dimensional correlation spectroscopy. *Fuel* **2024**, *359*, 130472.
(54) Xu, L. W.; Wang, C. Z.; Chang, H. Z.; Wu, Q. R.; Zhang, T.; Li, J. H. New insight into SO_2 poisoning and regeneration of CeO_2-WO_3/TiO_2 and V_2O_5-WO_3/TiO_2 catalysts for low-temperature NH_3-SCR. *Environ. Sci. Technol* **2018**, *52* (12), 7064−7071.
(55) Topsoe, N. Y.; Dumesic, J. A.; Topsoe, H. Vanadia-titania catalysis for selecitve catalytic reduction of nitric-oxide by ammonia. 2. Studies of active-sites and formulation of catalytic cycles. *J. Catal* **1995**, *151* (1), 241−252.
(56) Baron, M.; Abbott, H.; Bondarchuk, O.; Stacchiola, D.; Uhl, A.; Shaikhutdinov, S.; Freund, H. J.; Popa, C.; Ganduglia-Pirovano, M. V.; Sauer, J. Resolving the atomic structure of vanadia monolayer catalysts: monomers, trimers, and oligomers on ceria. *Angew. Chem., Int. Ed* **2009**, *48* (43), 8006−8009.
(57) Magg, N.; Immaraporn, B.; Giorgi, J. B.; Schroeder, T.; Bäumer, M.; Döbler, J.; Wu, Z. L.; Kondratenko, E.; Cherian, M.; Baerns, M.; Stair, P. C.; Sauer, J.; Freund, H. J. Vibrational spectra of alumina- and

https://doi.org/10.1021/acsomega.4c06372
ACS Omega 2025, 10, 358−367

silica-supported vanadia revisited: An experimental and theoretical model catalyst study. *J. Catal* **2004**, *226*, 88−100.
(58) Lewandowska, A. E.; Calatayud, M.; Tielens, F.; Banares, M. A. Hydration dynamics for vanadia/titania catalysts at high loading: a combined theoretical and experimental study. *J. Phys. Chem. C* **2013**, *117* (48), 25535−25544.
(59) Lewandowska, A. E.; Calatayud, M.; Tielens, F.; Banares, M. A. Dynamics of hydration in vanadia-titania catalysts at low loading: a theoretical and experimental study. *J. Phys. Chem. C* **2011**, *115* (49), 24133−24142.
(60) Rasmussen, S. B.; Portela, R.; Bazin, P.; Avila, P.; Banares, M. A.; Daturi, M. Transient operando study on the NH_3/NH_4^+ interplay in V-SCR monolithic catalysts. *Appl. Catal., B* **2018**, *224*, 109−115.
(61) Wu, R.; Li, L.; Zhang, N.; He, J.; Song, L.; Zhang, G.; Zhang, Z.; He, H. Enhancement of low-temperature NH_3-SCR catalytic activity and H_2O & SO_2 resistance over commercial V_2O_5-MoO_3/TiO_2 catalyst by high shear-induced doping of expanded graphite. *Catal. Today* **2021**, *376*, 302−310.
(62) Lian, Z.; Deng, H.; Xin, S.; Shan, W.; Wang, Q.; Xu, J.; He, H. Significant promotion effect of the rutile phase on V_2O_5/TiO_2 catalysts for NH_3-SCR. *Chem. Commun* **2021**, *57* (3), 355−358.

https://doi.org/10.1021/acsomega.4c06372
ACS Omega 2025, 10, 358−367